Evaluation of Cool Flame Characteristics of Droplet Pairs with Two-dimensional Calculation

Shion Ando*[1], Kenshin Koyama[1], Hiroya Tanaka[1], Osamu Moriue[1]
[1]Department of Mechanical Engineering, Kyushu University, Fukuoka, Japan
*Corresponding author email : ando-shion@mech.kyushu-u.ac.jp

Abstract
To investigate characteristics of cool and hot flame ignition of n-heptane droplet pairs with different sizes, 2-D numerical simulations were conducted. The initial droplet diameters were 0.4 mm and 1.0 mm, and spacing between the droplet centres (S_d) were 3 and 6 mm. The ambient temperature was 750 K, and the pressures were 0.1 and 0.3 MPa. Under each condition, cool flame ignition and two stage ignition were observed, respectively. When the pressure was 0.1 MPa and S_d was 3 mm, cool flame ignition occurred near the smaller droplet, resulting in cool flame apperance near the larger droplet. However, when S_d was 6 mm, each droplet independently showed cool flame ignition and subsequent appearance of cool flame around the larger droplet was not observed. At 0.3 MPa, because the diffusion of fuel vapor was mitigated, cool flame ignition independently occurred even if S_d was 3 mm. Regarding the hot flame, it occurred between the droplets regardless of S_d, which is probably due to the duplicated fuel source. The hot flame ignition occurred near the larger droplet, not in the middle point between the droplets. This is probably due to the larger Stefan flow from the smaller droplet.

Keywords
Droplet ignition, Cool flame, Hydrocarbon, Numerical simulation

Introduction

Isolated droplet combustion has been extensively investigated because it provides significant knowledge on spray combustion. Especially, under microgravity, effects of buoyancy was mitigated and heat and mass are transported spherically symmetrically, which makes it easy to model the phenomena. Since the classical theory on droplet combustion was constructed by Spalding and Godsave[1],[2], droplet combustion was theoretically and experimentally explored. Effects of unsteady phenomenon which are not included in the classic theory was theoretically considered[3],[4]. In addition, a lot of experiments have also been conducted to validate the theory[5],[6]. One of the most important findings of droplet combustion is the cool flame and two-stage ignition. Hydrocarbon fuel gases are widely known to exhibit cool flame with relatively low temperature (<1000 K) under certain conditions[7],[8]. After cool flame ignition, low-temperature oxidation reaction was supressed and instead hot flame ignition occurs. This is called as two-stage ignition. Tanabe et al. reported that hydrocarbon droplets such as n-dodecane also shows these phenomena[9],[10]. Additionally, Moriue measured cool flame and hot flame ignition of various alkane droplets, and showed that cool flame ignition delay mainly depends on volatility of fuels[11].

On the other hand, characteristics of spray combustion is largely influenced by the interaction between droplets. For example, Chiu et al. proposed to categorize the spray combustion by the number density of droplets, considering the effects between droplets[12]. Such an interaction cannot be evaluated by exploring isolated droplet combustion. Thus, droplet pairs and arrays have been widely investigated. Aminzadeh theoretically analysed sphere pair

combustion based on quasi-steady hypothesis and Schvab-Zeldovich formulation[13]. Umemura studied effects of interaction between droplets on the form of flame and burning rate by assuming that the mass flux can be expressed as a potential[14]. Experiments of droplet pair are mainly focused on the flame spread and subsequent combustion behaviour. Brzustowski et al. conducted combustion experiment of benzene droplet pair under microgravity[15]. Although they failed to measure the burning rate, it was reported that the flame shape changes depending on the distance between droplets. Miyasaka et al. measured the burning rate of two and three droplet array under convection[16]. Because the burning rate was not constant, they defined burning rate correction factor to evaluate the burning behaviour of droplet array. Later, Mikami et al. proposed to use modified burning rate correction factor, which also takes into account of unsteadiness of isolated droplet combustion[17]. By using this factor, they showed that instantaneous burning rate was first increased due to radiation and then decreased due to oxygen starvation. Recently, combustion of droplet pairs with different fuel[18] and biooils[19] have also been investigated.

These studies are focused on the combustion behaviour of droplet pair with the same initial diameter. However, actual spray is consisted of droplets with various diameter and this effects also should be clarified. Limited numbers of studies have been conducted on the combustion of droplet pair with different initial diameter. Similar to the previous study[14], Umemura et al. theoretically evaluated the flame shape and burning rate of droplet pair with different diameter by solving the potential equation on the mass flux[20]. As a result, they showed that the burning rate was smaller than that of isolated droplet and this tendency was more prominent for smaller droplet. Mikami et al. performed combustion experiment of n-decane droplet pair and clarified the relationship between the flame spread and droplet diameter / distance[21]. They discussed the flame spread time and rate in terms of the heating and heat conduction times. However, the study on the spontaneous ignition of droplet pair with different diameter is rather limited. Especially, characteristics of cool flame and two-stage ignition are not fully understood yet.

The objective of this study is to clarify the behaviour of cool flame and two-stage ignition of hydrocarbon fuel droplet pairs with different initial diameter. We have been experimentally explored the spontaneous ignition of hydrocarbon fuel droplet pairs under microgravity[22]. That study has revealed that cooling effects and duplicated fuel source has effects on the cool and hot flame ignition. When the initial droplet diameter is different, in addition to these effects, asymmetricity of velocity and concentration field would also have influences on the ignition. Numerical simulation was conducted for n-heptane droplets at 0.1-0.3 MPa and 750 K. Ambient gas comprised of 79% N2 and 21% O2.

Numerical Simulation

The numerical model and schemes applied in this study are described in this chapter. Numerical simulations of n-heptane droplet pairs were conducted with fully transient model. Droplets with room temperature were suddenly exposed in the high temperature ambience. And then, they begin to evaporate, ignite and combust.

Mass, momentum, energy and species conservation equations were solved in the gas phase. In the liquid phase, motions in the droplet were considered negligible, and only the heat conduction was considered. In addition, because it was assumed that droplet was composed of pure fuel, only energy conservation equation was solved in the liquid phase. Therefore, the governing equations were as follows,

Gas phase in the cylindrical coordinate:

$$\frac{\partial \rho}{\partial t}+\frac{1}{r}\frac{\partial}{\partial r}(r\rho u_r)+\frac{\partial}{\partial z}(\rho u_z)=0 \tag{1}$$

$$\frac{\partial \rho u_r}{\partial t}+\frac{1}{r}\frac{\partial}{\partial r}(r\rho u_r u_r)+\frac{\partial}{\partial z}(\rho u_r u_z)=-\frac{\partial p}{\partial z} \tag{2}$$

$$\frac{\partial \rho u_z}{\partial t}+\frac{1}{r}\frac{\partial}{\partial r}(r\rho u_z u_r)+\frac{\partial}{\partial z}(\rho u_z u_z)=-\frac{\partial p}{\partial z} \tag{3}$$

$$\begin{aligned}\rho C_{p_m}&\left(\frac{\partial T}{\partial t}+u_r\frac{\partial T}{\partial r}+u_z\frac{\partial T}{\partial z}\right)\\&=\frac{1}{r}\frac{\partial}{\partial r}\left(r\lambda\frac{\partial T}{\partial r}\right)+\frac{\partial}{\partial z}\left(\lambda\frac{\partial T}{\partial z}\right)\\&+\sum_{sp=1}^{spmax}\rho D_{sp}C_{p_{sp}}\left(\frac{\partial Y_{sp}}{\partial r}\frac{\partial T}{\partial r}+\frac{\partial Y_{sp}}{\partial z}\frac{\partial T}{\partial z}\right)-\sum_{sp=1}^{spmax}h_{sp}\omega_{sp}\end{aligned} \tag{4}$$

$$\rho\frac{\partial Y_{sp}}{\partial t}+\rho u_r\frac{\partial Y_{sp}}{\partial r}+\rho u_z\frac{\partial Y_{sp}}{\partial z}=\frac{1}{r}\frac{\partial}{\partial r}\left(r\rho D_{sp}\frac{\partial Y_{sp}}{\partial z}\right)+\frac{\partial}{\partial z}\left(\rho D_{sp}\frac{\partial Y_{sp}}{\partial z}\right)+\omega_{sp} \tag{5}$$

Gas phase in the spherical coordinate:

$$\frac{\partial \rho}{\partial t}+\frac{1}{r^2}\frac{\partial}{\partial r}(r^2\rho u_r)+\frac{1}{rsin\theta}\frac{\partial}{\partial \theta}(sin\theta\rho u_\theta)=0 \tag{6}$$

$$\frac{\partial \rho u_r}{\partial t}+\frac{1}{r^2}\frac{\partial}{\partial r}(r^2\rho u_r u_r)+\frac{1}{rsin\theta}\frac{\partial}{\partial \theta}(\rho u_r u_\theta)-\rho\frac{u_\theta^2}{r}=-\frac{\partial p}{\partial r} \tag{7}$$

$$\frac{\partial \rho u_\theta}{\partial t}+\frac{1}{r^2}\frac{\partial}{\partial r}(r^2\rho u_\theta u_r)+\frac{1}{rsin\theta}\frac{\partial}{\partial \theta}(sin\theta\rho u_\theta u_\theta)+\rho\frac{u_r u_\theta}{r}=-\frac{1}{r}\frac{\partial p}{\partial \theta} \tag{8}$$

$$\begin{aligned}\rho C_{p_m}&\left(\frac{\partial T}{\partial t}+u_r\frac{\partial T}{\partial r}+\frac{u_\theta}{r}\frac{\partial T}{\partial \theta}\right)\\&=\frac{1}{r^2}\frac{\partial}{\partial r}\left(r^2\lambda\frac{\partial T}{\partial r}\right)+\frac{1}{r^2sin\theta}\frac{\partial}{\partial \theta}\left(sin\theta\frac{\partial T}{\partial \theta}\right)\\&+\sum_{sp=1}^{spmax}\rho D_{sp}C_{p_{sp}}\left(\frac{\partial Y_{sp}}{\partial r}\frac{\partial T}{\partial r}+\frac{1}{r^2}\frac{\partial Y_{sp}}{\partial \theta}\frac{\partial T}{\partial \theta}\right)-\sum_{sp=1}^{spmax}h_{sp}\omega_{sp}\end{aligned} \tag{9}$$

$$\begin{aligned}\rho\frac{\partial Y_{sp}}{\partial t}&+\rho u_r\frac{\partial Y_{sp}}{\partial r}+\frac{\rho u_\theta}{r}\frac{\partial Y_{sp}}{\partial \theta}\\&=\frac{1}{r^2}\frac{\partial}{\partial r}\left(r^2\rho D_{sp}\frac{\partial Y_{sp}}{\partial r}\right)+\frac{1}{r^2sin\theta}\frac{\partial}{\partial \theta}\left(sin\theta\rho D_{sp}\frac{\partial Y_{sp}}{\partial \theta}\right)+\omega_{sp}\end{aligned} \tag{10}$$

Liquid phase:

$$\rho C_{p_m}\frac{\partial T}{\partial t}=\frac{1}{r^2}\frac{\partial}{\partial r}\left(r^2\lambda\frac{\partial T}{\partial r}\right)+\frac{1}{r^2sin\theta}\frac{\partial}{\partial \theta}\left(sin\theta\frac{\partial T}{\partial \theta}\right) \tag{11}$$

The equations in the gas phase were derived based on the low Mach number approximation. Soret and Dufour effects, radiation, viscosity and surface tension were not considered. Gas was treated as ideal gas. Transport and thermal properties of mixture gas were evaluated

based on the NASA polynomials. Heat conductivities in the gas and liquid phases were evaluated based on the method of Eucken and Latini methods[23], respectively. Pressure-velocity coupling was solved with SMAC method.

Droplet diameter was calculated as follows. From the species and mass continuities on the droplet surface, the following equation is derived.

$$-\frac{\rho_g D_g}{1-Y_{fg}}\left(\frac{\partial Y_f}{\partial r}\right)_g = \frac{1}{L_f}\left\{\lambda_g\left(\frac{\partial T}{\partial r}\right)_g - \lambda_l\left(\frac{\partial T}{\partial r}\right)_l\right\} = \dot{m}_{evap} \quad (12)$$

Here, the mole fraction of fuel on the droplet surface is calculated as a function of the surface temperature by assuming the vapor liquid phase equilibrium. Therefore, after the temperature and mass fraction in the gas and liquid phases were obtained, the droplet surface temperature was calculated using Eq. (12). After the droplet surface temperature was obtained, the evaporation mass flux is calculated from the middle and right-hand sides of Eq. (12). The droplet volume and diameter were calculated by integrating over the droplet surface at each time step.

The computational domain and girds used in this study are shown in Fig. 1. Natural convection was neglected, and the flow was assumed to be 2D axisymmetric. The height and width of the domain were 10 and 20 mm, respectively. The centres of both droplets were fixed and the distance between the droplet centres (S_d) was 4 mm. Initial droplet diameters were 0.4 and 1.0mm. The domain consisted of two types of coordinates. One of the coordinates was cylindrical coordinate which were located on the outer zone of the gas phase. In this zone, 100×200 rectangular grids were deployed. The other coordinate was spherical coordinate which were located in the gas phase near the droplet and liquid phase. In the liquid phase, grids were arranged regularly in the radial and angular directions. In the gas phase, grids which expands exponentially in the radial direction were arranged to make fine grids near the droplet surface.

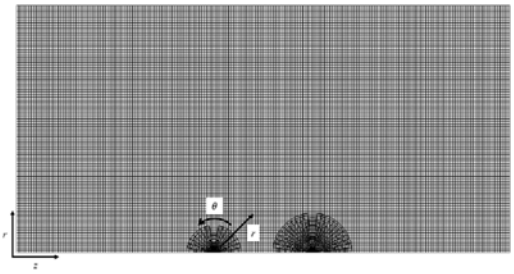

Figure 1. Computational domain employed in the simulation.

The numbers of the grids were 18 and 26 in the angular direction around the small and large droplets. In the radial direction, 10 grids were deployed in the gas phase and 15 and 20 grids were deployed in the small and large droplets, respectively. Cylindrical and spherical coordinates were connected with overset grid system. To avoid spurious oscillation of pressure, staggered grids were used to define the mass flux on the mesh interfaces. Free flow condition was applied for outer boundary conditions, and axisymmetric boundary condition was applied on the axis.

Discretization scheme was as follows. Convection term was discretized with first-order upwind difference, and other terms were discretized with second-order central difference. Although the time difference is explicit, only the chemical reaction was implicitly solved. A reaction mechanism for n-heptane (92 species, 437 reactions)[24] was used in this study.

Results and Discussion

First, cool flame ignition behaviour of n-heptane droplet pair was investigated at 0.1 MPa and 750 K. Because this chapter especially focuses on the cool flame behaviour, simulation was not conducted until the hot flame ignition. To clarify the effects of S_d, it is varied to 3 mm and 6 mm. Figure 2 shows the histories of distributions of temperature and temperature rise rate (CgT). In both cases, the temperature around the droplets decreased immediately after the beginning of calculation due to evaporation. After a while, CgT increased near the smaller droplet, which showed the occurrence of cool flame. Interestingly, cool flame ignition was observed at the left side of the smaller regardless of S_d. This is probably because the temperature decreases between the droplets due to the cooling effects of both droplets. Therefore, the left side of the smaller droplet was more likely to ignite than the right side. After cool flame ignition, it readily led to appearance of cool flame at right side and near the larger droplet. In the case of S_d of 6 mm, the cool flame appeared at the right side of smaller droplet, but it did not lead to appearance near the larger droplet. The smaller droplet was surrounded by the cool flame, and then the cool flame ignition occurred near the larger droplet. In this case, cool flame ignition of larger droplet homogeneously and spherically occurred, which suggests that the temperature field around the larger droplet became homogeneous after the cool flame ignition delay of smaller droplet.

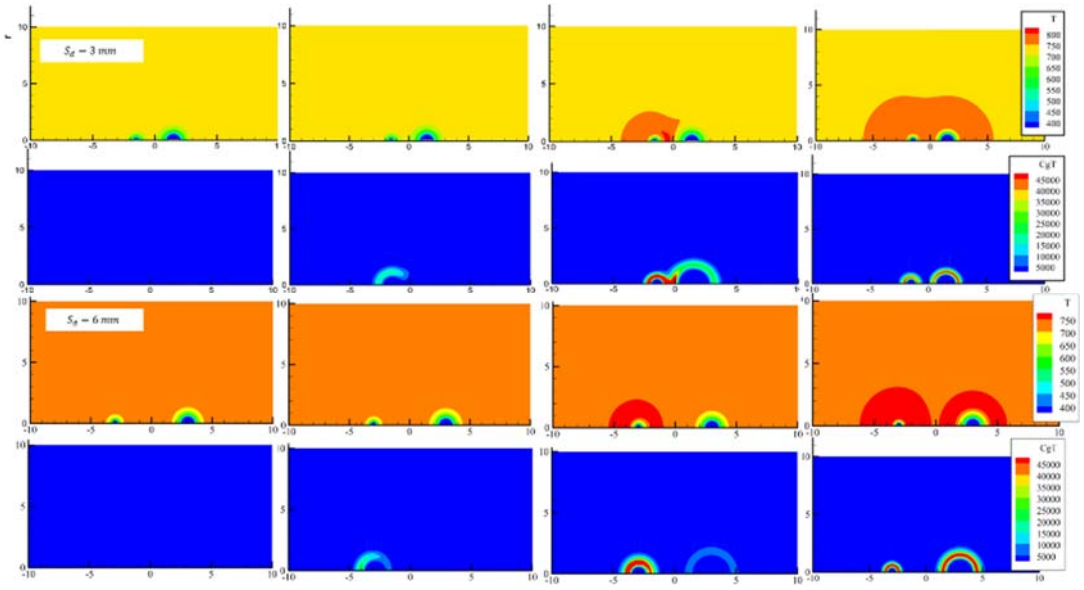

Figure 2. Histories of distributions of temperature and CgT at 0.1 MPa and 750 K. Upper: Sp=3mm, Lower: Sp=6mm.

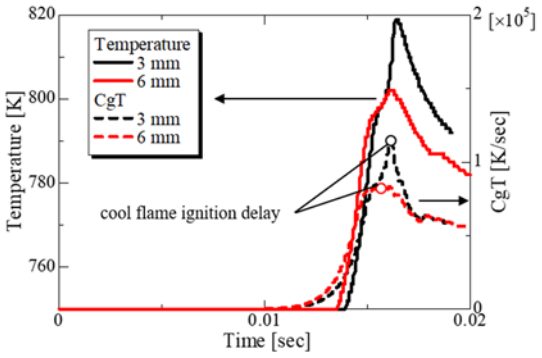

Figure 3. Histories of Maximum temperature and CgT at 0.1 MPa and 750 K. Circle shows the cool flame ignition delay.

Next, cool flame ignition delay was investigated. In this study, cool flame ignition delay was defined as the time when CgT temporarily showed the maximum value[24]. Figure 3 shows the histories of the highest temperature and CgT in the gas field. As shown in Fig.3, the difference of the cool flame ignition delay was small even if S_d was changed. This suggests that the temperature and fuel concentration at the left side of the smaller droplet were not affected by S_d. Generally, it is well known that cool flame characteristics is largely dependent on the temperature and concentration fields. Here, to explore the effects of temperature and fuel concentration on the cool flame ignition delay, characteristic chemical rate is investigated. Characteristics chemical rate is the reciprocal of the cool flame ignition delay at a certain temperature and equivalence ratio which is calculated by 0-D homogeneous ignition calculation. Figure 4 shows the distributions of characteristic chemical rate. As shown in Fig.4, when S_d was 3 mm, the characteristic chemical rate is larger at the left side of the smaller droplet, which correspond with the cool flame ignition behaviour mentioned above. For the case of S_d of 6 mm, the characteristic chemical rate showed almost spherical distribution around the smaller droplet. However, although the difference is small, the left side of smaller droplet showed higher characteristic chemical rate, which would lead to the cool flame ignition from the left side.

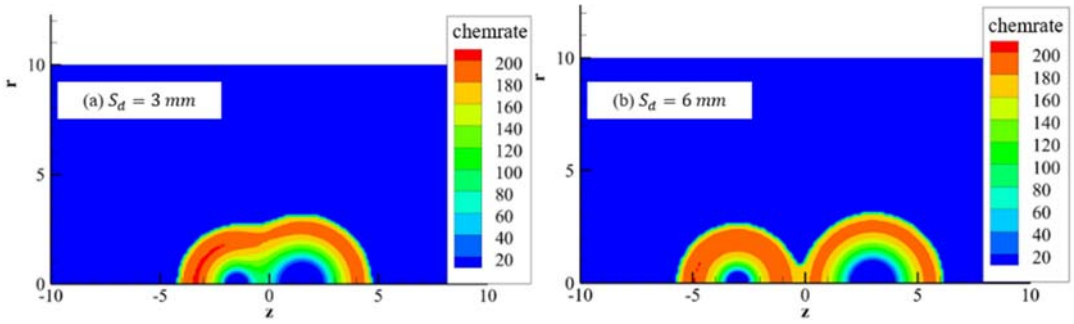

Figure 4. Distributions of characteristic chemical rate right before cool flame ignition at 0.1 MPa and 750 K.

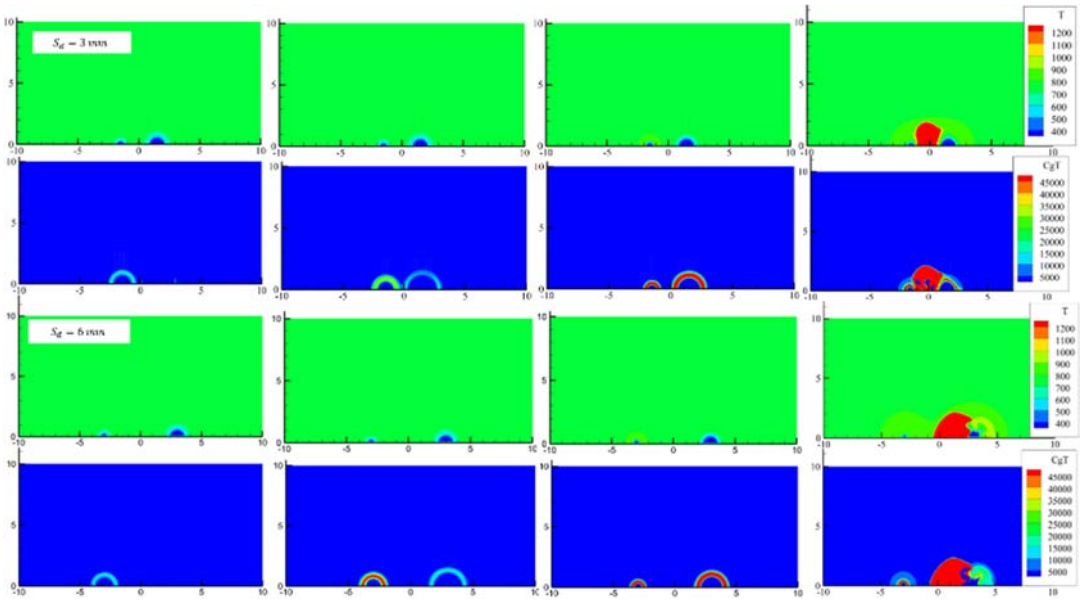

Figure 5. Histories of distributions of temperature and CgT at 0.3 MPa and 750 K. Upper: Sp=3mm, Lower: Sp=6mm

To investigate the characteristics of two stage ignition, simulation was conducted at 0.3 MPa and 750 K. Figure 5 shows the histories of distribution of temperature and CgT fields. S_d was 3 and 6mm. Contrary to the case of 0.1 MPa, the cool flame ignition almost spontaneously occurred around the smaller droplet even if S_d was 3 mm. This suggests that diffusion of fuel vapor was mitigated at high pressure and cool flame ignition independently occurred around each droplet. After the cool flame ignition around the smaller droplet, it also occurred around the larger droplet. Near the larger droplet, cool flame first appeared at the left side and it subsequently appeared at the right side, which showed that cool flame around the small droplet had effects on the cool flame appearance near the larger droplet. After cool flame appearance of large droplet, both droplets were surrounded by cool flame for a while. And then, hot flame ignition occurred between the droplets. The location of hot flame ignition is not the midpoint between the droplets but closer to the larger droplet. This might be due to the larger Stafan flow from the smaller droplet surface. Because mass flux of fuel vapor is larger for smaller droplets, hot flame ignition did not occur near the smaller droplet. Instead, it occurred near the stagnation point of the Stafan flow. Therefore, it can be concluded that hot flame ignition is largely affected not only by temperature and concentration fields but also by the flow fields.

Conclusions

To clarify the effects of S_d and atmosphere on the ignition behaviour of droplet pairs, numerical simulation of n-heptane droplets with different sizes were conducted at 0.1 and 0.3 MPa, 750 K. Droplet spacing was 3 and 6mm, and initial droplet diameters were 0.4 and 1.0 mm. The main conclusions are summarized below:

1. At 0.1 MPa and 750 K, when S_d was 3 mm, cool flame ignition was observed at outer side of the smaller droplet, subsequently causing cool flame appearance near the large droplet. This is probably because the temperature between the droplet became lower due to evaporation and cool flame ignition was likely to occur at the left side of the droplet.
2. At 0.1 MPa and 750 K, when S_d was 6 mm, cool flame ignition of each droplet independently occurred. In other words, smaller droplet was first surrounded by the cool flame and later, cool flame appeared around the larger droplet.
3. At 0.3 MPa and 750 K, cool flame ignition occurred almost spontaneously and spherically even if S_d was 3 mm. This is probably due to the inhabitation of diffusion of fuel vapor at high pressure.
4. Contrary to cool flame. hot flame was first observed between the droplets, which might be due to the duplicated fuel source.
5. The location of hot flame ignition was not at the midpoint between droplets but closer to the larger droplet. This is probably because the Stefan flow is larger for smaller droplet and stagnation point is located near the larger droplet.

Nomenclature

ρ	density [kg m^{-3}]
u	velocity [m s^{-1}]
p	pressure [kg m^{-1} s^{-2}]
Cp	constant pressure specific heat [J kg K]
T	temperature [K]
λ	heat conductivity [W m^{-1} K^{-1}]
D	diffusion coefficient [m^2 s^{-1}]
X	mole fraction [-]
Y	mass fraction [-]

h specific enthalpy [J mol^{-1}]
ω reaction rate [mol m^{-3} s^{-1}]
R gas constant [J kg^{-1} K^{-1}]
L latent heat of evaporation [J kg^{-1}]
$\dot{m}_{evap}$ evaporation mass flux [kg m^{-2} s^{-1}]

References

[1] Spalding, D. B., 1953, *Symposium (International) on Combustion*, *4* (1) pp. 847–864.
[2] Godsave, G. A. E., 1953, *Symposium (International) on Combustion*, *4* (1) pp. 818–830.
[3] Law, C. K.,Chung, S. H.,Srinivasan, N., 1980, *Combustion and Flame*, *38* (C) pp. 173–198.
[4] Matalon, M.,Law, C. K., 1983, *Combustion and Flame*, *50* pp. 219–229.
[5] S.Kumagai., 1956, *Jet Propulsion*, *26* (9) pp. 786–790.
[6] Kadota, T.,Hiroyasu, H.,Farazandehmehr, A., 1977, *Combustion and Flame*, *29* pp. 67–75.
[7] Pfahl, U.,Fieweger, K.,Adomeit, G., 1996, pp. 781–789.
[8] M.J. Pilling., "*Low-Temperature Combustion and Autoignition*," Elsevier Science, 1999, .
[9] Tanabe, M.,Kono, M.,Sato, J.,Koenig, J.,Eigenbrod, C.,Rath, H. J., 1994, *Symposium (International) on Combustion*, *25* (1) pp. 455–461.
[10] Tanabe, M.,Kono, M.,Sato, J.,Koenig, J.,Eigenbrod, C., Dinkelacker, F.,Rath Zarm, H. J., 1995, *Combustion Science and Technology*, *108* (1–3) pp. 103–119.
[11] Moriue, O.,Eigenbrod, C.,Rath, H. J.,Tsue, M.,Kono, M.,Sato, J., 2004, *Transactions of the Japan Society for Aeronautical and Space Sciences*, *47* (157) pp. 189–194.
[12] Chiu, H, H.,Liu, T, M., 1977, *Combustion Science and Technology*, *17* (3–4) pp. 127–142.
[13] Aminzadeh, K.,Al Taha, T. R.,Cornish, A. R. H.,Kolansky, M. S.,Pfeffer, R., 1974, *International Journal of Heat and Mass Transfer*, *17* (12) pp. 1425–1436.
[14] Umemura, A.,Ogawa, S.,Oshima, N., 1981, *Combustion and Flame*, *41* pp. 45–55.
[15] Brzustowski, T. A.,Twardu, E. M.,Wojcicki, S.,Sobiesiak, A., 1979, *AIAA Journal*, *17* (11) pp. 1234–1242.
[16] Miyasaka, K.,Law, C. K., 1981, *Symposium (International) on Combustion*, *18* (1) pp. 283–292.
[17] Mikami, M.,Kato, H.,Sato, J.,Kono, M., 1994, *Symposium (International) on Combustion*, *25* (1) pp. 431–438.
[18] Eigenbrod, C.,Wagner, V.,Paa, W., 2020, *Proceedings of the Combustion Institute*, *38* (2) pp. 1–9.
[19] Wang, J.,Zhang, H.,Zhang, Q.,Qiao, X.,Wang, X.,Ju, D.,Sun, C., 2021, *Fuel*, *285* (119077).
[20] Umemura, A.,Ogawa, S.,Oshima, N., 1981, *Combustion and Flame*, *43* pp. 111–119.
[21] Mikami, M.,Motomatsu, N.,Nagata, K.,Yoshida, Y.,Seo, T., 2018, *Combustion and Flame*, *193* pp. 76–82.
[22] Moriue, O.,Nishiyama, Y.,Yamaguchi, Y.,Hashimoto, H.,Murase, E., 2013, *Proceedings of the Combustion Institute*, *34* (1) pp. 1585–1592.
[23] Robert, C, R.,John, M, P.,Bruce, E, P., "*The Properties of Gases and Liquids*," 4th ed., McGraw-Hill International editions, 1988, .
[24] Schnaubelt, S.,Moriue, O.,Coordes, T.,Eigenbrod, C.,Rath, H. J., 2000, *Proceedings of the Combustion Institute*, *28* (1) pp. 953–960.